ML-Assisted Empirical Modeling with Blockage-Aware Attenuation for Sub-6 GHz Private 5G Using 3D City Maps and Satellite Imagery

Takuma Matsumoto* and Takeo Fujii*
* Advanced Wireless and Communications Research Center (AWCC), The University of Electro-Communications
1-5-1 Chofugaoka, Chofu, Tokyo 182-8585, Japan
Emails: {matsumoto,fujii}@awcc.uec.ac.jp

***Abstract*—Private 5G deployments often coexist in shared spectrum, motivating accurate yet lightweight prediction of received/interference power for inter-operator interference coordination. We propose a hybrid interference estimator for sub-6 GHz private 5G that combines a site-general empirical baseline with site-specific corrections derived from public geospatial data. The estimator integrates (i) an empirical baseline anchored to dominant distance dependence, (ii) a CNN–MLP residual correction using satellite imagery and 3D city maps, and (iii) a blockage-aware attenuation term for NLOS links computed from 3D city-map geometry, incorporating diffraction and proximity-reflection effects. To avoid a fully black-box model, the learning component estimates only the site-specific residual ΔP relative to the baseline, while distance dependence and blockage-induced NLOS propagation are retained in the physical/empirical components. Outdoor measurements show that the proposed method reduces the underestimation rate (OVRT) while maintaining or improving RMSE/MAE/STD compared with conventional approaches, at practical computational cost.**

I. Introduction

Because private 5G deployments often coexist in shared spectrum, network planning requires inter-operator interference coordination. A key input to coordination is the predicted received power (or path loss) over a service area, which determines separation distances, guard margins, and candidate deployment locations. In practice, received power is frequently predicted using lightweight, site general models that ignore local obstructions; conservative separation distances are then imposed, reducing spectrum efficiency [1]. High-fidelity methods such as ray tracing can improve accuracy by explicitly modeling interactions with buildings and terrain, but they incur substantial computational cost and are often impractical for large-scale or iterative planning. Conversely, many empirical models capture distance-dependent path-loss trends but require site-specific calibration to reflect local morphology and blockage conditions [2].

This paper addresses the accuracy–efficiency gap by combining data-driven and physics-based components. Specifically, we improve prediction accuracy without excessive overhead by integrating (i) an empirical baseline anchored to the dominant distance dependence, (ii) a learned residual correction that injects site-specific environmental factors inferred from satellite imagery and 3D city maps, and (iii) a blockage-aware attenuation model computed from 3D city-map geometry for NLOS links, incorporating diffraction and proximity-reflection effects. By using public geospatial data and lightweight computations, the proposed approach targets practical deployment scenarios where many candidate links must be evaluated under limited computation budgets.

II. Proposed Method

A. Overview: Processing Flow for LOS and NLOS Links

Fig. 1 first classifies each TX–RX link as LOS or NLOS using only 2D footprint intersection tests and 3D height lookups in the city map. After the classification, received power is estimated by selecting one of the following branches:

- **LOS branch** We estimate the LOS received power by an ML-assisted empirical model. An extended-Hata baseline captures the dominant distance dependence, while a CNN–MLP predicts RU-specific residual parameters $(\Delta C, \Delta\alpha)$ from RU-surrounding imagery and 3D-map-derived height features. The corrected path loss is $\hat{L}_{\mathrm{est}}(d) = \hat{L}_{\mathrm{base}}(d) + \Delta L_{\mathrm{pred}}(d)$, yielding $\widehat{P}_{r,\mathrm{LOS}}(d) = P_{\mathrm{EIRP}} - \hat{L}_{\mathrm{est}}(d)$.
- **NLOS branch** We start from the LOS estimate $\widehat{P}_{r,\mathrm{LOS}}$ and explicitly model blockage-induced excess attenuation. Using 3D map geometry, we search a diffraction path around obstructing objects and compute the single knife-edge diffraction loss $J(\nu)$. In addition, we optionally add a proximity reflection gain G_r when non-blocking structures exist near the receiver. The NLOS received power is then $\widehat{P}_{r,\mathrm{NLOS}} = \widehat{P}_{r,\mathrm{LOS}} - J(\nu) + G_r$.

This design keeps the computation lightweight: LOS relies on a fixed baseline plus an RU-conditioned residual model, while NLOS adds only map-derived diffraction/reflection terms when blockage is detected.

B. LOS/NLOS Classification with 3D Maps

Our method first determines whether the target estimation point is in LOS or NLOS with respect to the RU. We

project the TX–RX segment onto 2D and test intersections with building footprints; for each intersection at distance ratio $\alpha \in (0,1)$, we compare the path height $z(\alpha)$ with the building height $H(\alpha)$. LOS holds if $z(\alpha) > H(\alpha)$ for all intersections; otherwise NLOS. This requires only polygon–segment tests and height lookups; the complexity is $O(N_b)$ with N_b intersected footprints.

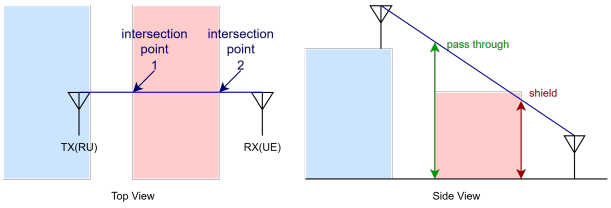

Fig. 1. Lightweight LOS/NLOS classification using 3D city maps.

C. Received Power in LOS: Machine Learning Assisted Empirical Model

1) Inputs and Metadata: Inputs for training and inference are: (i) field measurements (RU ID, receiver coordinates, and Reference Signal Received Power(RSRP)[dBm]), (ii) RU metadata (e.g., RU ID, system category, RU location, transmit power, antenna gain, etc.), (iii) RU-surrounding satellite/aerial imagery, and (iv) a 3D city model around the RU. These are obtained from: (i) PCTEL Gflex scanning-receiver measurements, (ii) licensing information and RU catalog specifications, (iii) aerial photographs provided by the Geospatial Information Authority of Japan (GSI), and (iv) PLATEAU 3D city models.

2) Distance-Dependent Trend: Fixed Extended-Hata Baseline: The dominant distance dependence is preserved by an extended Hata model without any environment-category correction. Training and inference always use this baseline as the anchor. The baseline path-loss model is

$$\hat{L}_{\mathrm{base}}(d) = 46.3 + 33.9\log_{10}(f_{\mathrm{MHz}}) - 13.82\log_{10}(h_b) - a(h_r) + \big(44.9 - 6.55\log_{10}(h_b)\big)\log_{10}(d_{\mathrm{km}}), \tag{1}$$

where f_{MHz} is the carrier frequency in MHz, d_{km} is the TX–RX distance in km, h_b is the RU antenna height, h_r is the receiver antenna height, and $a(h_r)$ is the receiver-height correction term.

3) Residual Definition in the Path-Loss Domain: Measured RSRP is mapped to measured path loss as

$$L_{\mathrm{meas}} = P_{tx} - \mathrm{RSRP}_{\mathrm{meas}}. \tag{2}$$

The learning target is the excess loss (residual) over the baseline:

$$\Delta L_{\mathrm{true}} = L_{\mathrm{meas}} - \hat{L}_{\mathrm{base}}. \tag{3}$$

This decomposition keeps distance dependence in the baseline and assigns environment dependence to the residual.

4) Extraction of Environmental Features: For each RU, we construct a 4-channel tile by combining RU-surrounding satellite imagery (RGB) with a depth/height channel derived from the 3D city map (e.g., building height above ground). The tile is reshaped and normalized. A CNN acts as an environment feature extractor: it compresses the 4-channel tile into a compact embedding vector that summarizes site characteristics (e.g., building density, vegetation/open areas visible in imagery, and 3D obstruction patterns captured by the depth/height channel).

5) Training: The ML module predicts RU-specific parameters $\theta_{\mathrm{RU}} = [\Delta C, \Delta\alpha]$. The residual is modeled as

$$\Delta L_{\mathrm{pred}}(d) = \Delta C + \Delta\alpha \log_{10}(d_{\mathrm{km}}), \tag{4}$$

where ΔC is an RU-specific bias and $\Delta\alpha$ adjusts the residual slope versus log-distance. Measurement points are grouped by RU, and train/validation splits are performed at the RU level. CNN+MLP parameters are optimized to minimize the MAE between ΔL_{pred} and ΔL_{true} over all measurement points. Training is repeated for 60–100 epochs and the best model is saved.

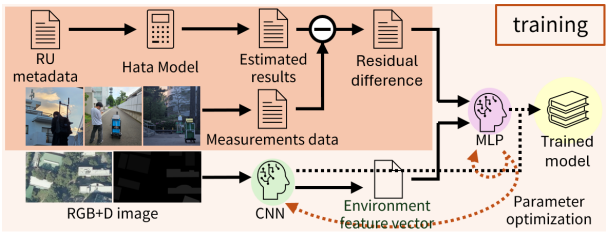

Fig. 2. Training process of the ML-assisted empirical model.

6) Inference: Corrected Path-Loss Estimation: Given satellite imagery, the 3D city model, and RU metadata around the target site, the model estimates $(\Delta C, \Delta\alpha)$. For any distance d,

$$\hat{L}_{\mathrm{est}}(d) = \hat{L}_{\mathrm{base}}(d) + \Delta L_{\mathrm{pred}}(d), \tag{5}$$

and the LOS received power is estimated as

$$\widehat{P}_{r,\mathrm{LOS}}(d) = P_{\mathrm{EIRP}} - \hat{L}_{\mathrm{est}}(d), \tag{6}$$

where P_{EIRP} denotes the RU EIRP. In this paper, we evaluate P_r using RSRP.

This yields a predicted curve (path loss / received power) as a function of distance.

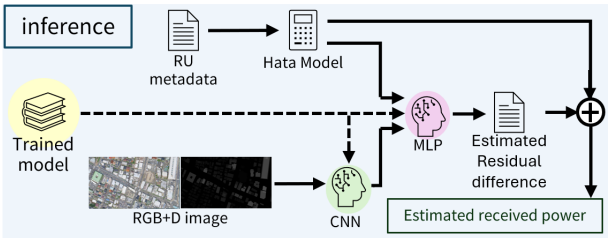

Fig. 3. Inference process of the ML-assisted empirical model.

D. Received Power in NLOS: Blockage-Aware Attenuation Model

1) Path Estimation: For obstructing objects, we compute the shortest TX–RX path that passes along the object edges while remaining unblocked.

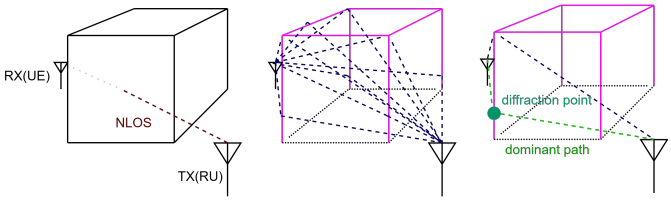

Fig. 4. Search diffraction path around obstructing objects.

2) Blockage-Induced Effects: We add the ITU-R single knife-edge diffraction loss $J(\nu)$ and a proximity reflection gain G_r:

$$\widehat{P}_{r,\mathrm{NLOS}} = \widehat{P}_{r,\mathrm{LOS}} - J(\nu) + G_r, \tag{7}$$

where $\widehat{P}_{r,\mathrm{LOS}}$ is the received-power estimate from the LOS model.

Let d_1, d_2 be the distances from the knife-edge to TX/RX and h the clearance above the straight line joining TX and RX (negative if below). With wavelength λ, the Fresnel diffraction parameter is [3]:

$$\nu = h\sqrt{\frac{2}{\lambda}\left(\frac{1}{d_1}+\frac{1}{d_2}\right)} = \sqrt{\frac{2}{\lambda}}\,\frac{h\sqrt{d_1+d_2}}{\sqrt{d_1 d_2}}. \tag{8}$$

The knife-edge diffraction loss $J(\nu)$ (dB) is approximated by:

$$J(\nu) = \begin{cases} 0, & \nu \le -0.78, \\ 6.9+ \\ 20\log_{10}\left(\sqrt{1+(\nu-0.1)^2}+\nu-0.1\right), & \nu > -0.78. \end{cases} \tag{9}$$

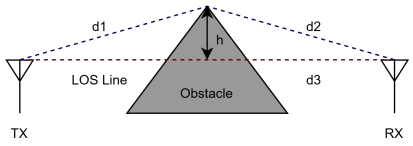

Fig. 5. Knife-edge diffraction model.

Empirically, reflections correlate with nearby wall distance; we add G_r when non-blocking structures exist within 10 m of the RX (e.g., $G_r = +5$ dB).

III. Experiments

A. Setup and Metrics

Outdoor trials used multiple experimental private-5G stations (Exp.) and multiple base stations of a commercial private-5G service (Com.) in an urban area. A PCTEL Gflex logged RSRP at each location with position and RU ID. TX power, antenna gains/heights, and other RU parameters were taken from operator-provided information and licensing information; these were provided as metadata together with the system type, and kept consistent within each system.

For the ML-assisted empirical component (LOS), RU-centric 4-channel tiles were formed by concatenating aerial RGB imagery and a height (depth) tile derived from PLATEAU CityGML [4]. Tiles were cropped around each RU, resized, and normalized. Training/validation used RU-level LOEOCV (leave-one-environment-out cross-validation), holding out all samples of one RU to test generalization to unseen sites.

For blockage-aware attenuation in NLOS, 3D city-model data were converted to 2D building footprints with height attributes, aligned to the measurement coordinates, and used for LOS/NLOS judgment and blockage-impact calculations (e.g., diffraction and reflection).

Metrics are RMSE, MAE, and STD of the prediction error (dB), and the measured-over-estimate ratio (measured / estimated).

$$\mathrm{OVRT}(\%) = 100\,\frac{\#\{\, i \mid \hat{P}_{r,i} < P_{r,i} \,\}}{N}. \tag{10}$$

Smaller OVRT is preferable for interference protection. Baselines: the Ministry of Internal Affairs and Communications (MIC) private-5G model [1] and ITU-R P.1411 [5].

B. Results: LOS Path-Loss Estimation by an ML-Assisted Empirical Model

We collected measurements in 10 environments and evaluated the ML-assisted empirical model using RU-level LOEOCV, holding out all samples of one RU for testing and training on the remaining RUs. The ML component learns only the excess loss relative to a fixed baseline, $\Delta L_{\mathrm{true}} = (P_{tx} - \mathrm{RSRP}_{\mathrm{meas}}) - \hat{L}_{\mathrm{base}}$, from RU-centric 4-channel images (aerial RGB + depth/height from PLATEAU CityGML) and RU meta features.

Fig. 6 shows results for one of our RU sites - Fuda3NS, illustrating that the model compensates for an RSRP shift due to catalog–deployment mismatches and captures changes in the attenuation curve across site conditions.

Across the 10 environments ($N = 9604$ samples), Table I summarizes the RU-level LOEOCV results: the mean MAE improved from 37.04 dB (extended Hata without environment correction) to 7.57 dB (ML-assisted), and MAE improved in 9/10 environments, ranging from -2.16 dB to $+39.14$ dB. In contrast, the mean OVRT increased from 1.07% to 48.13% (decreased only in 2 environments), consistent with the baseline's positive bias being reduced toward near-zero bias by ML (Table I). Therefore, interference-protection use requires a conservative margin (e.g., a validation-calibrated global offset). The results suggest that many system type–Com RUs exhibit a substantial mismatch between the licensed (or nominal) transmit power and the actual radiated power. Even without environmental inputs, the ML model can estimate this mismatch, which appears to be a major contributor to the MAE reduction.

TABLE I
PER-ENVIRONMENT LOEOCV RESULTS OF THE ML-ASSISTED EMPIRICAL MODEL (LOS).

Env.	System	N	$\mathrm{MAE}_{\mathrm{base}}$ [dB]	$\mathrm{MAE}_{\mathrm{ML}}$ [dB]	ΔMAE [dB]	ΔMAE[%]	$\mathrm{OVRT}_{\mathrm{base}}$ [%]	$\mathrm{OVRT}_{\mathrm{ML}}$ [%]	ΔOVRT [pp]
Chofu2	Com.	1184	34.96	6.99	27.97	80.0	0.0	68.4	68.4
Fuda3EW	Com.	574	50.61	11.48	39.14	77.3	0.0	2.6	2.6
Fuda3NS	Com.	880	46.99	9.16	37.83	80.5	0.0	22.4	22.4
Fuda4	Com.	1018	27.18	9.83	17.35	63.8	0.0	88.8	88.8
Fuda6	Com.	1757	38.62	6.28	32.33	83.7	0.0	35.6	35.6
Kojima1	Com.	1378	39.67	8.81	30.85	77.8	0.0	9.5	9.5
Kojima3	Com.	2636	35.01	5.78	29.23	83.5	0.0	70.3	70.3
Kyutech	Exp.	29	12.37	8.89	3.48	28.2	6.9	41.4	34.5
NICTKoganei1	Exp.	67	8.16	10.31	-2.16	-26.5	65.7	62.7	-3.0
UEC	Exp.	81	7.05	5.00	2.05	29.0	70.4	39.5	-30.9
Overall		9604	37.04	7.57	29.47	79.6	1.1	48.1	47.1

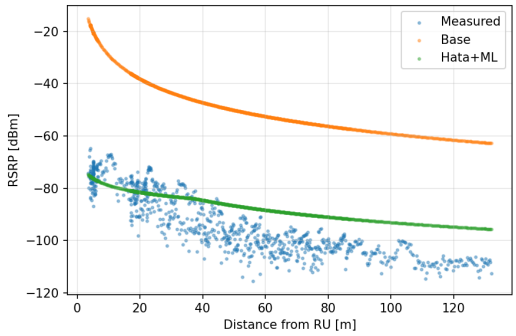

Fig. 6. Estimated vs. measured RSRP at Fuda3NS (LOS).

C. Results: NLOS Received-Power Estimation by the Blockage-Aware Attenuation Model

We evaluate the blockage-aware attenuation model under NLOS conditions at the UEC campus (RU height: 1.55 m). The NLOS received power is computed by adding diffraction loss and a proximity-reflection gain to the LOS estimate, explicitly capturing blockage-dependent attenuation. As shown in Fig. 7 and Table II, the proposed method improves RMSE/MAE/STD versus the MIC model and reduces OVRT (71.5% $\rightarrow$ 17.1%), implying fewer underestimations and safer interference coordination with smaller guard margins. Compared with ITU-R P.1411, RMSE/MAE are lower at UEC NLOS, while OVRT is not consistently reduced.

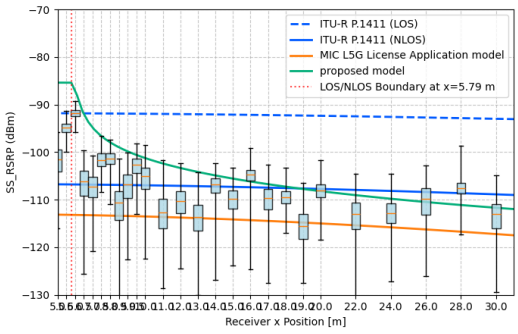

Fig. 7. Estimated vs. measured RSRP at UEC (NLOS).

TABLE II
STATISTICS AT UEC (NLOS).

Model	RMSE[dB]	MAE[dB]	STD[dB]	OVRT[%]
Proposed	7.57	5.87	5.58	17.1
ITU-R P.1411 (LOS / NLOS)	26.01 / 5.90	25.33 / 4.47	5.92 / 5.85	0 / 43.5
MIC	6.60	5.12	5.87	71.5

IV. EVALUATION

A. Contribution of Input Modalities to ML Performance

To investigate the contribution of the input data used by the ML model, we compared the MAE among the following settings: (i) without ML, (ii) with no environmental imagery (NoImage), (iii) with only building-height imagery (Depth), (iv) with only RGB imagery (RGB), and (v) with both RGB and depth imagery (RGBD). The results are shown in Fig. 8.

Compared with the ML model without environmental imagery (NoImage), the MAE change introduced by adding RGBD imagery ranged from a best-case improvement of 1.9 dB to a worst-case degradation of -1.1 dB, indicating that the environmental information was not effectively exploited for some RUs. In contrast, the results suggest that many system type–Exp RUs show a consistent MAE improvement in the order of: without ML, NoImage ML, and RGBD-input ML. Relative to NoImage ML, the MAE improvement gained by RGBD imagery was up to 7.4 dB and at least 0.8 dB. These results suggest that challenges remain in selecting and ensuring the quality of the input data provided to the model.

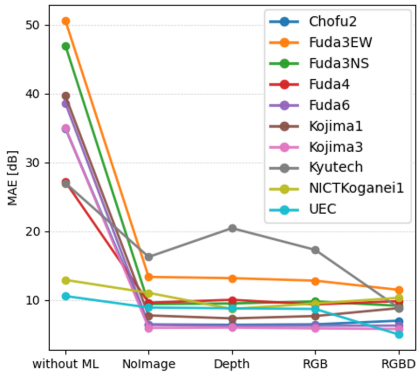

Fig. 8. Comparison of MAE across input modality settings (without ML, NoImage, Depth, RGB, and RGBD).

B. Computational Cost Comparison

Table III summarizes, for each scenario, the end-to-end runtime of the proposed model (Python, single CPU thread) and Remcom Wireless InSite's X3D ray tracing (RTX 4070 SUPER, 0.25° angular resolution, up to six reflections and one diffraction). Although X3D ray tracing is GPU-accelerated, it still incurs approximately 3×10^2 to 5×10^3 times higher computational cost than the proposed model in our experiments.

TABLE III
TOTAL RUNTIME OF THE PROPOSED MODEL AND WIRELESS INSITE X3D RAY TRACING, AND THEIR RATIO.

Scenario	N_{dist}	Proposed [ms]	X3D RT [ms]
Kyutech LOS	10^3	11.34	3.67×10^3
	5×10^3	18.15	8.69×10^3
	10^4	23.77	21.09×10^3
UEC LOS	10^3	10.71	11.56×10^3
	5×10^3	17.45	56.26×10^3
	10^4	24.98	126.44×10^3
UEC NLOS	10^3	11.98	4.27×10^3
	5×10^3	21.24	13.92×10^3
	10^4	32.14	39.64×10^3

C. Discussion on OVRT and Conservative Margin

According to the experimental results, although the proposed method reduces the overall prediction error, the underestimation rate, denoted by OVRT [%], increases, which is insufficient from an interference-mitigation perspective. This behavior stems from the training objective, which is designed to minimize the mean absolute error (MAE). Figure 9 compares the predicted and measured values (i.e., the ground-truth values) obtained by the proposed method and the conventional Hata model. From this comparison, it is confirmed that the proposed method reduces outlier-like errors while exhibiting an approximately symmetric error distribution centered around the ground-truth values regardless of the received power level. Therefore, when a conservative design is required, introducing a margin of 10–20 dB can reduce OVRT.

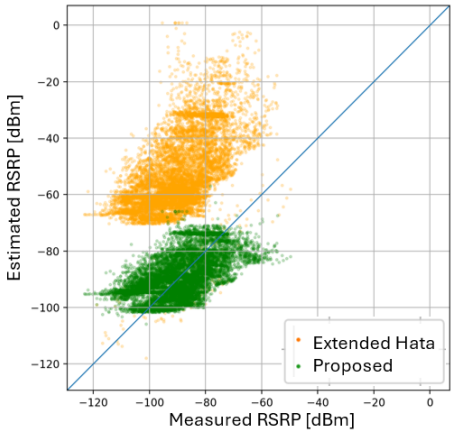

Fig. 9. Estimated vs. measured (ground-truth) RSRP.

V. CONCLUSION AND FUTURE WORK

We proposed a lightweight hybrid interference estimator for Sub-6 GHz private 5G by combining an extended-Hata baseline, an ML-based residual correction from RU-centric RGB+height tiles, and a 3D-map-based blockage model for NLOS. LOEOCV over 10 environments ($N = 9604$) reduced the mean MAE from 37.04 dB to 7.57 dB. For NLOS at UEC, the blockage model reduced OVRT from 71.5% to 17.1% versus the MIC model. Future work includes calibrating conservative margins for interference safety and extending the blockage modeling and validation.

ACKNOWLEDGMENT

This work includes results from the project "R&D for Expansion of Radio Spectrum Resources" funded by the Ministry of Internal Affairs and Communications, Japan (JPJ000254).

REFERENCES

[1] Ministry of Internal Affairs and Communications (MIC), "Private 5G License Application Support Manual," 2023. (in Japanese)
[2] V. Silva, R. Feick, L. Ahumada, R. A. Valenzuela, M. S. Derpich, and M. Rodríguez, "Empirical comparison of propagation models for relay-based networks in urban environments," *IEEE Access*, vol. 10, pp. 7313–7325, Jan. 2022.
[3] ITU-R, "Propagation by diffraction," *Recommendation ITU-R P.526-14 (01/2018)*, International Telecommunication Union, Geneva, Switzerland, 2018.
[4] G-Spatial Information Center, "3D City Model (Project PLATEAU) Portal," accessed Apr. 20, 2025. Available: https://front.geospatial.jp/plateau_portal_site
[5] ITU-R, "Propagation data and prediction methods for the planning of short-range outdoor radiocommunication systems and radio local area networks in the frequency range 300 MHz to 100 GHz," Rec. ITU-R P.1411-10, 2019.